

Ambient air synthesis of multi-layer CVD graphene film for low-cost, efficient counter electrode material in dye-sensitized solar cells

Dong Han Seo^{1†}, Munkhbayar Batmunkh^{2†}, Jinghua Fang³, Adrian T. Murdock¹, Sam Yick¹, Zhaojun Han¹, Cameron J. Shearer², Thomas J. Macdonald⁴, Malcolm Lawn⁵, Avi Bendavid¹, Joseph G. Shapter^{2*}, Ken Ostrikov^{6*}

† These authors contributed equally to this work.

¹ CSIRO Manufacturing, P.O. Box 218, Bradfield Road, Lindfield, NSW 2070, Australia.

² School of Chemical and Physical Sciences, Flinders University, Bedford Park, Adelaide, SA 5042, Australia.

³ School of Mathematical and Physical Sciences, The University of Technology, Sydney, NSW 2007, Australia

⁴ Department of Chemistry, University College London, 20 Gordon Street, London WC1H 0AJ, UK

⁵ National Measurement Institute, Nanometrology, 36 Bradfield Road, Lindfield, NSW 2070, Australia.

⁶ Institute for Future Environments and Institute for Health and Biomedical Innovation, School of Chemistry, Physics, and Mechanical Engineering, Queensland University of Technology, Brisbane, QLD 4000, Australia.

Correspondence and requests for materials should be addressed to Prof. Kostya Ostrikov and Prof. Joe Shapter (email: Kostya.Ostrikov@qut.edu.au and Joe.shapter@flinders.edu.au)

Abstract

Graphene holds great promise as a counter electrode (CE) material as a substitution to the conventional Pt in dye-sensitized solar cells (DSSCs). However, lengthy chemical processing with hazardous chemicals, high production cost, poor quality of graphene flakes produced and material intensive for device integration impedes their utilization as a CE material in DSSCs. Herein, we demonstrate low-cost synthesis of graphene film using a thermal chemical vapour deposition (CVD) process in ambient-air environment using renewable source such as soybean oil, for which no expensive compressed gases are needed. The utilization of our low-cost graphene film in DSSCs exhibits excellent electrocatalytic activity and high electrical conductivity, and thus delivers superior photovoltaic (PV) efficiency as compared to the devices fabricated with graphene films produced from commonly adopted chemical methods. Despite no additional treatment such as heteroatom doping is applied, our low-cost graphene showed great promise in DSSCs, which suggests that this material has the potential to be ideal CE material. Further enhancement in the efficiency of our graphene film based DSSCs is readily achievable by applying advanced functional treatments including heteroatom doping (for example SOCl_2). Finally, material cost analysis of our graphene film compared to commercial Pt electrode suggests that we can reduce the device manufacturing cost by five folds, making our CVD graphene film to be more favourably adopted commercially in DSSC system.

Keywords: Dye-sensitized solar cells, counter electrode, chemical vapor deposition, graphene, low-cost

1. Introduction

Dye-sensitized solar cell (DSSC) is under intensive development and has become a promising alternative photovoltaic (PV) system to the traditional crystalline silicon solar cells.^[1] In a typical high efficiency DSSC, a platinum (Pt) coated counter electrode (CE) plays an important role as electrocatalyst to in reducing I_3^- to I^- .^[2] However, the rarity and high cost of Pt electrocatalysts have led to a comprehensive amount of efforts being focused on finding alternative CE materials including those based on carbon nanomaterials such as carbon powder,^[3] carbon nanotubes (CNTs)^[4, 5] and graphene^[6]. Among them, graphene has attracted much attention owing to its highly tuneable properties and unique structure.^[7]

Although excellent progress has been made in the development of graphene CEs for DSSCs and many studies demonstrated comparable PV performance to the Pt electrode based devices,^[8-10] the methods used to fabricate these graphene based electrocatalysts usually involve several complicated production steps which lead to high manufacturing cost. For example, chemically derived graphene oxide (GO) and/or reduced graphene oxide (rGO) without additional modifications often show poor device performances when used in DSSC CEs, despite they involve lengthy chemical processes to produce the materials.^[11, 12] The limited conductivity and significant defects of the flakes introduced during the chemical processes are the main reasons for the poor device efficiencies. Therefore it is well established that heteroatom doping on the chemically derived graphene sheets is an excellent strategy to obtain high efficiency DSSCs,^[8-10, 13] but such doping process is complicated and requires extra cost. Alternatively, highly conductive graphene films produced using conventional chemical vapor deposition (CVD)

methods have been employed as CE materials in DSSCs, but these devices suffer from very poor power conversion efficiencies (PCEs) (only around 1%).^[14, 15] This is mainly due to the lack of catalytically active sites in these CVD-graphene sheets, despite they are produced at high synthesis cost using explosive purified gases. In this regard, developing a novel, low-cost strategy that can be used to produce highly conductive and catalytically active graphene nanosheets is of great importance.

In this work, we present a single-step, fast, low-cost ambient air synthesis of highly functional graphene film as an effective CE material for DSSCs. Our graphene film is prepared from a renewable bio-source such as soybean oil and notably, without the use of any expensive and explosive compressed gases.^[16] The DSSCs fabricated with our low-cost graphene (without any additional treatment) based CEs showed higher efficiency than the chemically derived graphene structures such as GO and rGO based devices. Further enhancement in the PCE of our graphene based DSSC is accomplished by applying simple treatment with SOCl_2 solution, making our low-cost graphene comparable to the Pt electrocatalyst for DSSCs. More importantly, we present material cost analysis of our graphene film compared to the commercial Pt electrode for DSSCs.

2. Results and Discussion

The conventional CVD process to produce graphene films requires long time annealing processes at high-temperatures, use of expensive and purified compressed gases and lengthy vacuum condition.^[17] To overcome such hurdles, we recently discovered a low-cost, single step,

unique thermal CVD strategy to prepare high-quality graphene film in an ambient-air environment that is completely free of compressed gases and only utilizes renewable sources such as soybean oil.^[16] Thermal dissociation of soybean oil in ambient air provided all the necessary building blocks for the graphene growth on a polycrystalline Ni substrate, and Ni acts as a catalysts to promote the growth of the graphene film. In this work, we also demonstrated effective control over graphene film thickness ranging from few ten nanometer to nearly 1 micrometer by adjusting the amount of soybean oil, annealing temperatures and cooling rates. It should be noted that achieving thick graphene film using the conventional CVD method is extremely challenging, which is one of the main limitations for its application in DSSC CEs. The experimental steps of graphene synthesis and film transfer onto fluorine-doped tin oxide (FTO) substrate are schematically illustrated in **Figure 1a-c**. It can be observed that the colour of reflective, metallic polycrystalline Ni foil is changed to greyish after the growth of multi-layer graphene film.

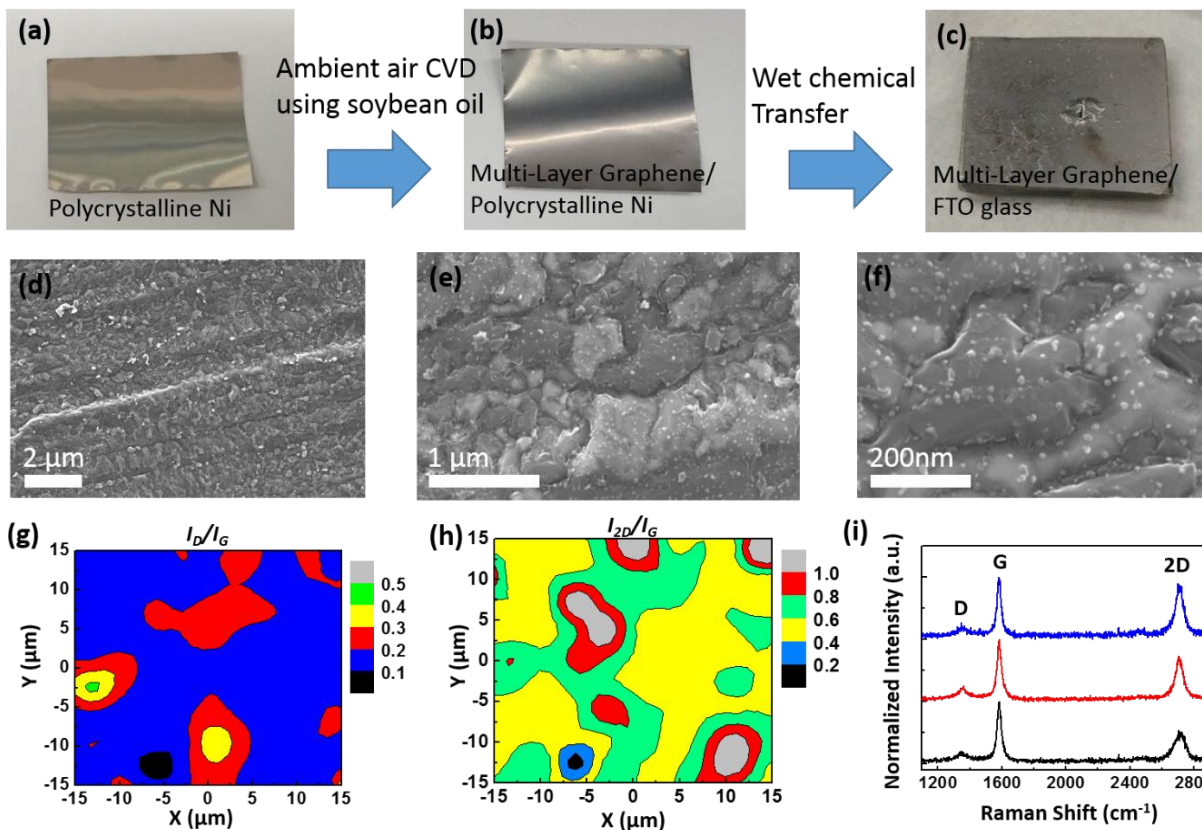


Figure 1. Multi-layer graphene film grown in an ambient-air environment using soybean oil for DSSC application. (a, b, c) Schematic illustration for the preparation of graphene CE for DSSC. (d, e, f) SEM images of multi-layer graphene on the FTO substrate. (g, h) Raman areal mapping of I_D/I_G and I_{2D}/I_G ratio and (i) Raman spectrum of our graphene film.

The morphological and structural properties of our graphene film were analyzed by a scanning electron microscopy (SEM) (**Figure 1d-f**) and Raman spectroscopy (**Figure 1g-i**). As shown in **Figure 1d-f** and **Figure S1**, the full coverage of graphene on FTO glass reveals rough surface with numerous polycrystalline graphene domains. Moreover, due to a turbo-static stacking of graphene domains with different thicknesses, permeable gaps can be observed between the

domains, which would be beneficial for the interaction of the electrolyte and graphene. A confocal Raman mapping further confirms that our graphene is a multi-layer sheets with polycrystalline domains. Raman spectral mappings based on the I_D/I_G and I_{2D}/I_G intensity ratios can be used to determine the defect level and thickness uniformity of the graphene films (**Figure 1g-h**).^[18] The intensity ratios of I_D/I_G ranged from 0.1 to 0.3, and the average I_D/I_G ratio was 0.15. Similarly I_{2D}/I_G ratio ranged from 0.2 to 1, while its average ratio was 0.5. The analysis of spectral mapping reveals that our graphene film contained low defect level with large variation in graphene thicknesses over large-area. Three distinct peaks located at $\sim 1350\text{ cm}^{-1}$, $\sim 1580\text{ cm}^{-1}$ and $\sim 2700\text{ cm}^{-1}$ can be observed from the Raman spectrum of our graphene film shown in Figure 1i. These characteristics peaks of graphene materials can be readily associated to the (i) disorder peak (D peak) which arises from the defects in the sp^2 carbon, (ii) graphitic peak (G peak) arises from the in-plane vibrational E_{2g} mode of the sp^2 carbon, and (iii) second-order 2D-band arises from the inter-planar stacking of hexagonal carbon network.^[19]

Similarly, transmission electron microscopy (TEM) analysis depicted in **Figure 2a-d** and **Figure S2**) shows polycrystalline, mis-oriented graphene domains with sizes ranging from $\sim 200\text{ nm}$ to $\sim 800\text{ nm}$. Different colour variations of the graphene domains in the TEM image reveal their thickness variations. Such observation was supported by selected area electron diffraction (SAED) pattern taken at different graphene domains (see **Figure 2b** and c). A distinct ring-like pattern was observed for the darker regions, while the lighter region showed much clear hexagonal pattern, suggesting the darker ad-layer region is thicker than the lighter base graphene layers. Notably, small degree of rotation was observed between the base layer and ad-layer.

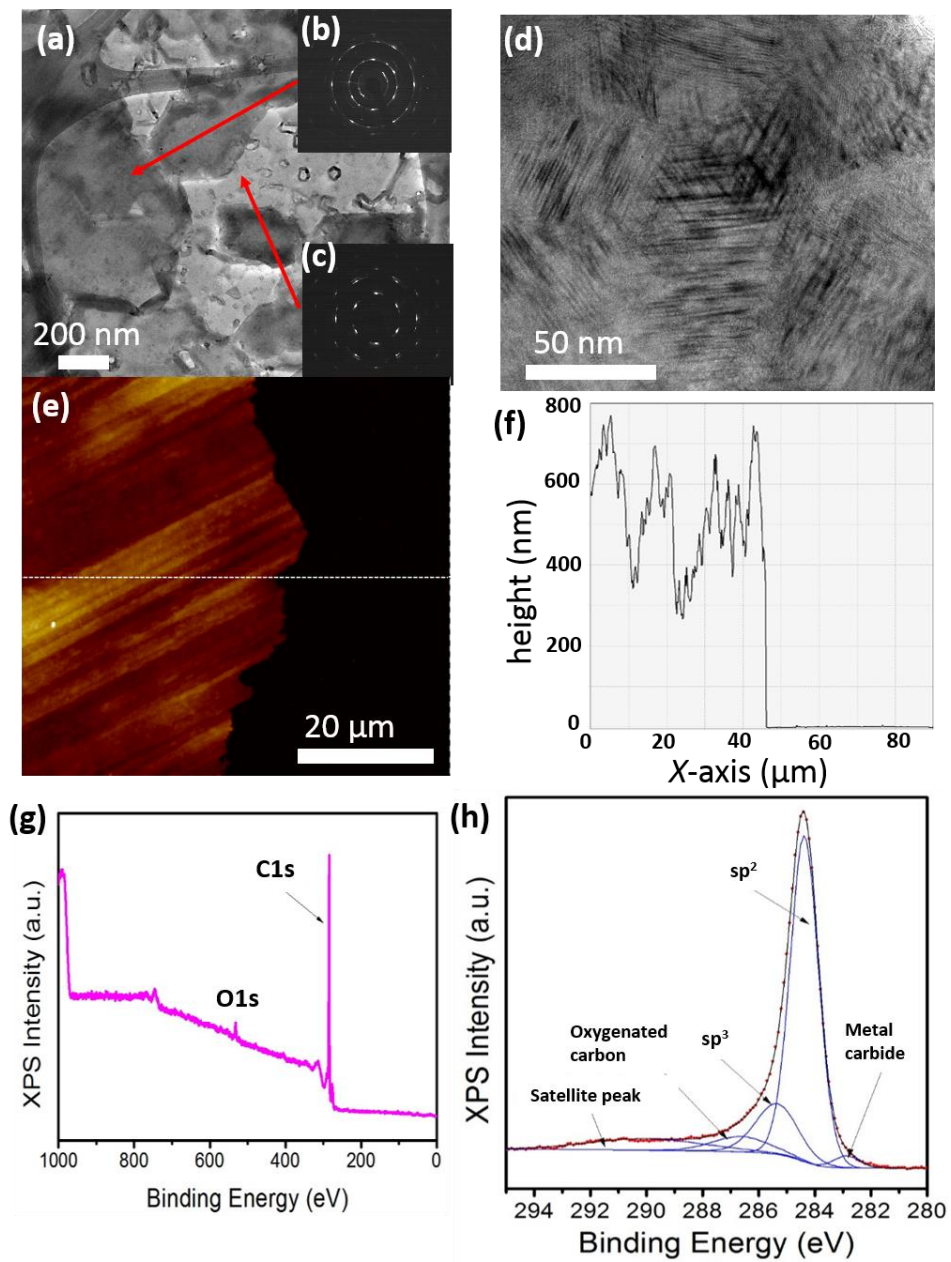


Figure 2. Atomic and nanoscopic features of the multi-layer graphene film synthesized from soybean oil for DSSC CEs. (a) TEM image, (b, c) SAED pattern, (d) high resolution TEM image, (e) AFM image and (f) corresponding height profile of our graphene film. (g) XPS survey scan and (h) C1s spectra of the multi-layer graphene film.

Atomic force microscopy (AFM) analysis shows that our graphene film had large variation in its thickness across the large-area (**Figure 2e** and **f**), with the thickness ranging from 300 nm to 700 nm and 450 nm for the average. Furthermore X-ray photoelectron spectroscopy (XPS) was carried out to provide an important information about the elemental composition and bonding nature of our graphene. The XPS survey scan (**Figure 2g**) shows a dominant narrow C1s peak at the binding energy of 284.5 eV and a weak O1s peak, demonstrating that our graphene is less oxidized which is in agreement with the Raman result. The C1s narrow scan (**Figure 2h**) was deconvoluted into five peak components, corresponding to sp^2 carbon (284.5 eV), sp^3 carbon (285.4 eV), metal carbide (282.8 eV), oxygenated carbon (286.5 eV) and satellite peak (~291 eV).^[20] Our graphene film exhibited high sp^2/sp^3 ratio of ~4, revealing the good structural quality of the graphene film. Overall, based on a diverse range of characterizations above, our low-cost graphene film synthesized using ambient air CVD method possess several important advantages including (i) continuous film with good structural quality and low defect level, which will provide high conductivity, 2) polycrystalline graphene with numerous domains with varying thicknesses which provide permeable gaps for the excellent electrolyte infiltration in DSSC devices.

An ideal CE material for DSSC should satisfy the following requirements: (i) good electrocatalytic activity, (ii) high conductivity, (iii) high surface area for the electrolyte infiltration, (iv) low-cost and (v) simple to produce. To explore the suitability of our graphene

electrodes as the CE materials in DSSCs, we fabricated DSSC devices based on our graphene and investigated their PV performance, electrocatalytic activity and charge-transfer properties.

The thickness of the graphene films plays a critical role in the PV performance of the devices. Therefore we fabricated DSSCs with three different thicknesses of graphene CEs. The film thickness was adjusted in this work by changing the synthesis parameters such as precursor amount, temperature and cooling rate.^[21, 22] The devices fabricated with different thickness were labelled as T1, T2 and T3 which correspond to ~40 nm, ~450 nm and ~750 nm, respectively (see **Figure 2e** and **f**, and **Figure S3**). The photocurrent density-voltage (J-V) characteristics of the DSSCs fabricated with T1, T2 and T3 electrodes are shown in **Figure S4** and the corresponding PV parameters such as short-circuit current (J_{sc}), open-circuit voltage (V_{oc}), fill factor (FF) and PCE have been summarized in **Table S1**. Indeed the optimum PV parameters were achieved for the T2 graphene CE (450 nm) based DSSC device, which was selected for further investigation. For comparison, we also prepared chemically derived graphene structures including GO and rGO as CE materials for DSSCs. A precious metal Pt electrocatalyst was also used as the reference.

To explore the electrocatalytic activity of these CE materials for the liquid triiodide based DSSC system, cyclic voltammetry (CV) measurements were carried out with a three-electrode system. These CE materials were labelled with different colour lines in **Figure 3a**. Two typical peaks corresponding to the oxidation and reduction of triiodide electrolytes are observed from the CV measurements (see **Figure 3b**). The left pair (i) at the lower potential can be attributed to the oxidation and reduction of I^-/I_3^- , while the right pair (ii) at the higher potential corresponds to

those of I_3^-/I_2 .^[23] In general, higher peak current density and lower peak to peak separation (E_{pp}) indicates higher catalytic activity of the materials.^[5, 8] As shown in **Figure 3b**, the Pt electrocatalyst displays the highest peak current density and lowest E_{pp} , indicating that precious Pt is still the best CE material for triiodide reduction. In contrast, a very poor catalytic activity was observed for the GO sample which is unsurprisingly due to its extremely low conductivity caused by the presence of heavy oxygen containing functional groups. On the other hand, both rGO and our graphene electrodes showed improved peak current density and E_{pp} . However, the E_{pp} value of the rGO was lower than that of our graphene, indicating that the electrocatalytic activity of rGO is slightly higher than that of our graphene. This is probably due to the defective sites introduced during the chemical oxidation and reduction processes of graphene nanosheets. It is well understood that these defective sites can act as electrocatalytically active sites for the triiodide reduction in DSSCs.^[5, 10, 13, 24] Interestingly, our graphene exhibited higher peak current density as compared to the rGO, revealing better conductor.

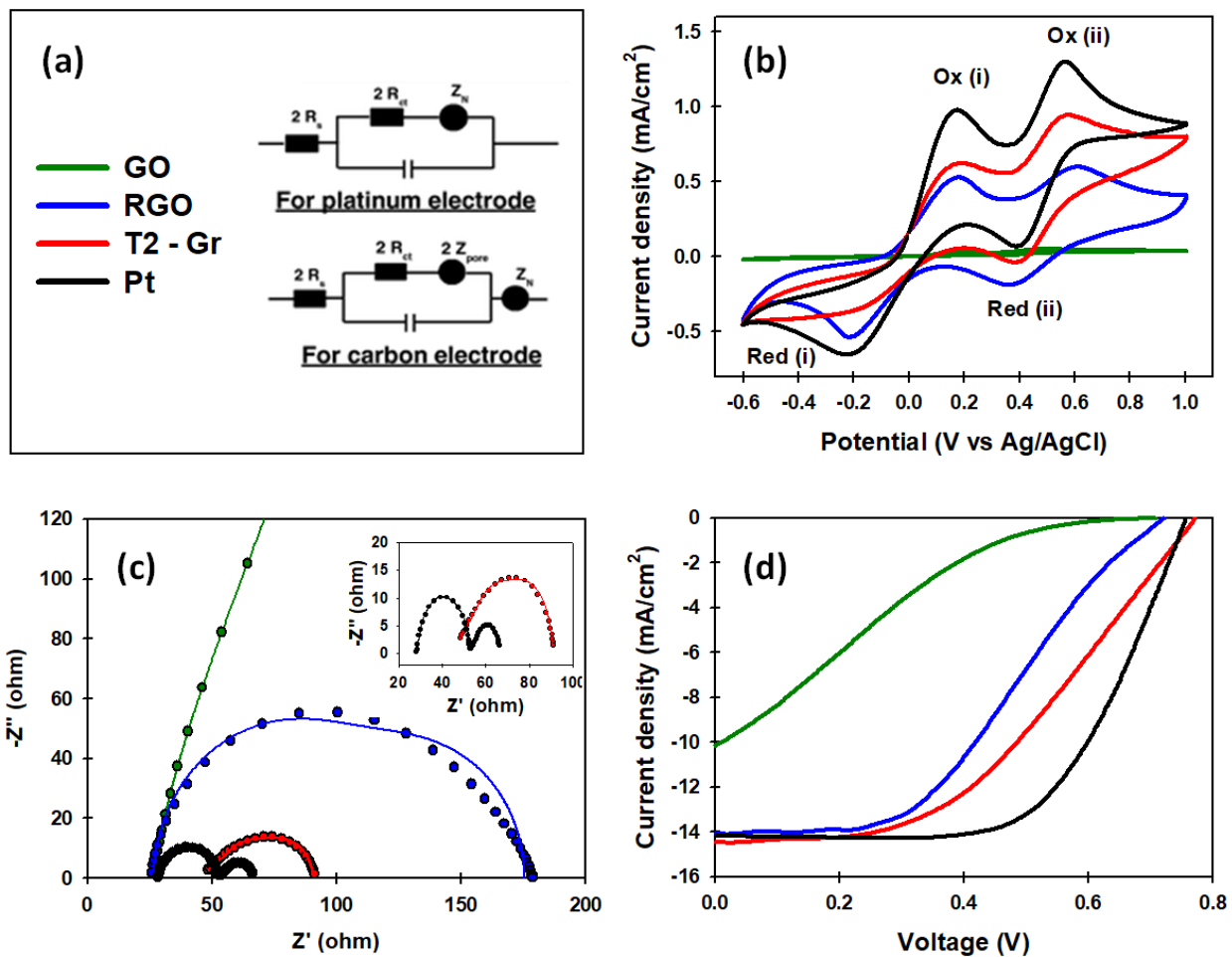


Figure 3. (a) sample labelling (left) and Equivalent circuit diagrams for EIS analysis (right). (b) Cyclic voltammograms (CVs), (c) EIS spectra and (d) J-V curves of the GO, RGO, our low-cost graphene and Pt based CE materials and their DSSC devices.

To evaluate the charge-transfer properties of these CE materials, electrochemical impedance spectroscopy (EIS) was recorded for the dummy cells consisting of a symmetrical sandwich structure (electrode/ I^-/I_3^- electrolyte)/electrode). The Nyquist plots illustrated in **Figure 3c** were obtained by fitting the experimentally measured EIS data to a modelled equivalent circuit

diagram (**Figure 3a**, right). The charge-transfer resistance (R_{ct}) of the electrode materials can be measured from the corresponding Nyquist plots and the values are listed in **Table 1**. Because of its poor conductivity, the R_{ct} of the GO was very high (4.4 k Ω). Our graphene showed an R_{ct} of 20.8 Ω , which was \sim 4.5 times lower than that (93.4 Ω) of the rGO. The lowest R_{ct} (15.6 Ω) was obtained for the Pt cells. These EIS results were in good agreement with the CV measurements.

Table 1. PV parameters of the DSSCs fabricated based on different CE materials.

Sample	J_{sc} (mA cm ⁻²)	V_{oc} (V)	FF	PCE (%)	R_{ct}
GO	10.10	0.71	0.17	1.22	4.4 k Ω
rGO	14.06	0.72	0.42	4.29	93.4 Ω
T2 – Gr	14.45	0.77	0.44	4.95	20.8 Ω
Pt	14.19	0.76	0.62	6.66	15.6 Ω

Furthermore, DSSCs were fabricated based on these four CEs and their J–V characteristics are depicted in **Figure 3d**. Detailed PV parameters of these cells have been summarized in Table 1. As expected, the device with GO electrode exhibited a very poor PCE due to the insulating nature of GO material. After the partial reduction of GO, the PV parameters were significantly improved and a PCE of 4.29% was achieved for the rGO based DSSC. Interestingly, our low-cost graphene CE based DSSC showed higher efficiency (4.95%) than that of the rGO based device. In

particular, the measured J_{sc} , V_{oc} and FF of our T2 – Gr based device were 14.45 mA cm⁻², 0.77 V and 0.44, respectively. On the other hand, our control device fabricated with Pt CE exhibited a PCE of 6.66%. It should be noted that although the R_{ct} of our graphene was comparable to that of the Pt, its PV performance was considerably lower than the Pt based DSSC. It can be clearly seen from Table 1 that the lower FF value of our graphene based device was the main reason for achieving lower PCE as compared to the Pt based cell. The poor FF value of our graphene based DSSC is mainly due to the lack of electrocatalytically active sites on the nanosheets. Despite this, the PV performance observed for our low-cost graphene based DSSC can be considered as an impressive result since there was no additional treatment such as heteroatom doping was applied on our graphene.

It is very well established that the functionalization of graphene nanosheets is a powerful strategy to obtain high efficiency DSSCs.^[6] Doping with heteroatoms is known excellent method to enhance the PV performance of graphene CEs based DSSCs.^[25] Therefore we anticipate that significant enhancement in the efficiency of our low-cost graphene CE based DSSC can be achieved by employing further functionalization strategies. As an example, we employed SOCl₂ treatment to introduce some doping effect onto our graphene sheets. The SOCl₂ doping is widely used approach to enhance the conductivity of nanocarbon materials.^[26] The PV characteristics, electrocatalytic and charge-transfer properties of our graphene CE based DSSC before and after SOCl₂ treatment are summarized in **Figure S5** and **Table S2**. A clear enhancement in the FF value was observed after the SOCl₂ treatment and thus resulted in an improved PCE. This enhancement in the FF value was due to the improved electrocatalytic activity and reduced R_{ct} of our graphene CE after treating with SOCl₂, which were confirmed by

both CV and EIS measurements (see **Figure S5**). However, we observed reduction in the V_{oc} value after treating with $SOCl_2$ which is probably due to the changes in the energy level of our graphene introduced by the $SOCl_2$ doping. Although our $SOCl_2$ treated graphene showed lower R_{ct} (11.3 Ω) than the Pt (15.6 Ω), the PCE of our graphene based DSSC (5.53%) was slightly lower than that of the precious Pt based device (6.66%). This is reasonable because the electrocatalytic active sites on our graphene nanosheets even after $SOCl_2$ treatment are still insufficient to obtain comparable or higher efficiency as compared to the Pt. Despite this, our work provides an excellent demonstration to produce extremely low-cost graphene CEs and opens a new avenue for the development of Pt-free DSSCs. Further improvement in the efficiency is still expected by applying effective heteroatom doping such as sulphur, nitrogen and phosphorus.

To gain further insight on the economic viability of employing our low-cost CVD graphene, we performed material cost comparison between our graphene CE and commercial Pt precursor based CE (see Table S3). Material cost analysis shows that even at our small production scale, we can reduce the manufacturing cost of DSSC by 5 folds by using our CVD graphene instead of precious Pt CE. Therefore, it is expected to be lower if the manufacturing is scaled up. The key reason for this low-cost graphene synthesis is the fact that the use of cheap renewable source to completely avoid using expensive purified gas components. Moreover, fast processing time also provides low electricity cost to produce our graphene.^[16]

Conclusion

In summary, we have demonstrated low-cost, compressed gas-free CVD synthesis of graphene film in ambient air environment derived from renewable source such as soybean oil for CE material in DSSCs. As compared to the chemically derived graphene structures such as GO and rGO, our graphene CE based device showed significantly higher PCE despite no additional treatment was employed. Moreover, chemical functionalization treatment using SOCl_2 on our graphene CE further enhanced the PV performance of DSSC due to the reduced R_{ct} and improved electro-catalytic activity. Furthermore, material cost comparison of our graphene CE and Pt based CE suggested that we can reduce the manufacturing cost of DSSC by 5 folds by using our graphene based CEs. This work provides an important example to prepare low-cost graphene electrocatalysts and opens a new research avenue for the development of less expensive DSSCs.

Experimental Section

Ambient air CVD synthesis of thickness controlled polycrystalline, multi-layer graphene film from soybean oil

The growth of multi-layer graphene film with different thickness was carried out in a thermal CVD furnace with a quartz tube. Polycrystalline Ni foils (30 μm , 99%, MTI) were used as the growth substrates. To obtain the multi-layer graphene film with optimum thickness (for T2 – Gr sample, average thickness of graphene film $\sim 450\text{nm}$), 0.25 mL of soybean oil precursor was

placed on the alumina boat and polycrystalline Ni foil was placed near the soybean oil precursor. Then the openings of the quartz tube were sealed. The temperature of 800 °C for 3 min was used to grow the multi-layer graphene film. After the annealing process, the sample was cooled to room temperature. During the heating processes, atmospheric pressure was maintained in the quartz tube by releasing the pressure through the tube exhaust. No compressed gases were used at any stage of the experiment. To synthesize the thicker graphene film (T3 – Gr sample, average thickness of graphene film ~ 750nm), the amount of precursor and the annealing temperature was adjusted. Particularly, 0.3 mL of soybean oil was used and the growth temperature was increased to 900°C. After 3 min annealing, the sample was cooled down to room temperature. Similarly, to obtain the thinner graphene film (T1 – Gr sample, average thickness of graphene film ~40nm), low amount of precursor was used with fast cooling rate. In particular, 0.18 mL of soybean oil was used and the annealing temperature was 800°C. After 3 min annealing, the chamber was evacuated, followed by another 3 min and fast quenching. Then the sample was cooled down to room temperature.

Transfer of graphene

A poly (methyl methacrylate) (PMMA)-assisted transfer of graphene was adopted. Briefly, 46 mg/mL of PMMA (M_w 996,000 Sigma-Aldrich) was spin-coated onto the graphene/polycrystalline Ni foil at 3000 rpm for 1 min, followed by drying in an open air. Then the underneath Ni foil was dissolved in 0.4 M $FeCl_3$. The PMMA/graphene film then was transferred onto a FTO coated glass, followed by washing with deionized water. The PMMA was

then dissolved in acetone and the sample was rinsed with ethanol. For the SOCl_2 treatment, after the transfer process of graphene onto the FTO glass substrate, SOCl_2 solution (Sigma Aldrich) was dropped onto the graphene film.

Preparation of GO and rGO electrodes

Graphene oxide (GO) was prepared via the oxidation and exfoliation of natural graphite according to an improved Hummers method reported by Marcano et al.^[27] Briefly, a 9:1 (v:v) mixture of sulfuric acid (95–98% H_2SO_4) and phosphoric acid (85% H_3PO_4) (240:27 mL) was kept in the cold (3–5°C) until it was added to a mixture of graphite flakes (2 g) and potassium permanganate (99% KMnO_4) (12 g). The oxidation process of graphite was carried out by stirring the mixture at ~50 °C for 12 h. Then, the reaction was cooled down to room temperature and poured onto ice (300 mL) with 30% hydrogen peroxide (H_2O_2) (2 mL). The mixture was then washed with distilled (DI) water, 30% hydrochloric acid (HCl) and ethanol (x 2 times). For each sequential wash, the product was centrifuged at 4400 rpm for 3 h and the supernatant decanted away. The light brown sample obtained was dispersed and exfoliated in an aqueous solution, and then freeze-dried to obtain GO powder.

The reduction of GO to produce rGO was carried out at 900 °C for 3 h with a heating rate of 5 °C min^{-1} . The calcination process includes five steps: 1) purge the tube furnace with N_2 gas at room temperature for 30 min, 2) increase the temperature to 120 °C, 3) Hold at 120 °C for 2 hr to remove moisture in the GO, 4) Increase the temperature to 900 °C, 5) Hold at 900 °C for 3 hrs, followed by cooling down to room temperature.

The well established procedures described in Mayhew et al.^[24] was used to prepare viscous paste. Ethyl cellulose was used as an adhesive binder for the pastes. The prepared pastes were sonicated for 5 min before use and then deposited onto the cleaned FTO electrodes via a doctor blade technique, followed by drying in an oven at 90 °C for 5–10 min and annealing at 420 °C for 20 min. For comparison, Pt CEs were prepared by coating Pt precursor onto FTO substrates using a brush–painting method, followed by platinizing at 450 °C for 20 min.

Device fabrication

Firstly FTO coated glass electrodes were cleaned sequentially using detergent, DI water, acetone and finally ethanol. The cleaned FTO substrates were immersed into a 40 mM aqueous TiCl_4 solution at 90 °C for 15 min, and rinsed with water and ethanol. Then, ~10 μm thick TiO_2 layer (Dyesol 18NR–T, transparent) was deposited on the FTO electrodes by a doctor blading. The TiO_2 films were gradually heated under an air flow at 125 °C for 5 min, 325 °C for 5 min, at 375 °C for 15 min and at 500 °C for 30 min, followed by cooling to room temperature. Then, ~6 μm thick light scattering TiO_2 layer (Dyesol WER2–O) was printed on the transparent TiO_2 layer. The electrodes were sintered at 500 °C for 1 h. After sintering, the electrodes were immersed in aqueous TiCl_4 (40 mM) solution at 90 °C for another 15 min, followed by final annealing at 500 °C for 1 h. After cooling to room temperature, the prepared TiO_2 electrodes were immersed into 0.5 mM N719 dye in an ethanol solution for 18 h at. The dye adsorbed TiO_2 electrodes and previously prepared CEs were assembled into a sealed sandwich–type cells, with a 60 μm thick hot–melt sealing Surllyn between each layer. The electrolyte solution, Iodolyte Z–50 (Solaronix),

was introduced into the cell via a vacuum–filling method through an injection hole on the CE side. Finally, the hole was sealed with scotch tape.

Characterization

Raman spectroscopy was performed using a Renishaw inVia spectrometer with Ar laser excitation at 514 nm and a probing spot size of about $1 \mu\text{m}^2$. Atomic force microscopy (AFM) images were acquired with an Asylum Research MFP-3D AFM operating in intermittent contact (“tapping”) mode with a 5 N/m spring constant cantilever. Image analysis was performed using the Scanning Probe Image Processor (SPIP™) software produced by Image Metrology A/S. Transmission electron microscopy (TEM) was performed using a JEOL 2200FS TEM microscope operated at 200 kV. X-ray photoelectron spectroscopy (XPS) spectra were conducted with a Specs SAGE 150 spectroscope with Mg K α excitation at 1253.6 eV. Both survey scans and narrow scans of C 1s was conducted. SEM images were taken using ULTRA-ZEISS SEM microscope operated at 5kV.

Both CV and EIS measurements were performed using an electrochemical analysis workstation (Autolab Nova Potentiostat). The CV was carried out in a three electrode system with different CE materials as the working electrode, a Pt wire as the counter electrode, and Ag/Ag⁺ electrode as the reference electrode, at a scan rate of 50 mV s^{-1} . The electrodes were dipped in an anhydrous acetonitrile solution containing 10 mM LiI, 1 mM I₂, and 0.1 M LiClO₄. EIS measurements were analyzed by means of the Z–view software.

The photocurrent–voltage (J – V) characteristics were analyzed using a Keithley 2400 SMU instrument and recorded using a custom LabView Virtual Instrument program. A standard

silicon test cell with NIST-traceable certification was used to calibrate the power density as 100 mW cm⁻² at the sample plane of the collimated a 150W xenon–arc light source (Newport), which was passed through an AM 1.5G filter. The active area of the fabricated devices was 0.19 cm².

Acknowledgements

This work was supported by the Australian Research Council (ARC) and CSIRO's OCE Science Leadership Program. D.H.S, A.T.M, and S.Y. acknowledge the CSIRO's OCE Postdoctoral Fellowship Program. J.H.F. acknowledges the DECRA Fellowship from the ARC. Z.J.H. and K.O. acknowledge the support from the ARC and CSIRO research office respectively. The use of South Australian node of the Australian Microscopy & Microanalysis Research Facility (AMMRF) and Australian National Fabrication Facility (ANFF) at Flinders University is acknowledged. The support of the Australian Research Council Discovery Program (DP150101354 and DP160101301) is gratefully acknowledged.

Supplementary information

Supplementary Information is available from the Wiley Online Library and request to the corresponding author.

Competing financial interests

A PCT patent has been filed for this invention, PCT/AU2016/050738, Commonwealth Scientific and Industrial Research Organisation (CSIRO) on 12 August 2016 under title "AMBIENT AIR GRAPHENE SYNTHESIS" by Dong Han Seo, Shafique Pineda, Zhaojun Han and Kostya Ostrikov.

References

- [1] M. Batmunkh, M. J. Biggs, J. G. Shapter, *Adv. Sci.* **2015**, 2, 1400025.
- [2] S. Yun, A. Hagfeldt, T. Ma, *Adv. Mater.* **2014**, 26, 6210.
- [3] A. Kay, M. Grätzel, *Sol. Energ. Mat. Sol. Cells.* **1996**, 44, 99.
- [4] M. Batmunkh, M. J. Biggs, J. G. Shapter, *Small.* **2015**, 11, 2963.
- [5] A. Shrestha, M. Batmunkh, C. J. Shearer, Y. Yin, G. G. Andersson, J. G. Shapter, S. Qiao, S. Dai, *Adv. Energy Mater.* **2017**, 7, 1602276.
- [6] H. Wang, Y. H. Hu, *Energy Environ. Sci.* **2012**, 5, 8182.
- [7] J. D. Roy-Mayhew, I. A. Aksay, *Chem. Rev.* **2014**, 114, 6323.
- [8] E. Bi, H. Chen, X. Yang, W. Peng, M. Gratzel, L. Han, *Energy Environ. Sci.* **2014**, 7, 2637.
- [9] A. G. Kannan, J. Zhao, S. G. Jo, Y. S. Kang, D.-W. Kim, *J. Mater. Chem. A.* **2014**, 2, 12232.
- [10] X. Meng, C. Yu, X. Song, Y. Liu, S. Liang, Z. Liu, C. Hao, J. Qiu, *Adv. Energy Mater.* **2015**, 5, 1500180.
- [11] M. Batmunkh, A. Shrestha, G. Gao, L. Yu, J. Zhao, M. J. Biggs, C. J. Shearer, J. G. Shapter, *Sol. RRL.* **2017**, 1, 1700011.
- [12] H. Fang, C. Yu, T. Ma, J. Qiu, *Chem. Commun.* **2014**, 50, 3328.
- [13] X. Meng, C. Yu, X. Song, Z. Liu, B. Lu, C. Hao, J. Qiu, *J. Mater. Chem. A* **2017**, 5, 2280.
- [14] S. Das, P. Sudhagar, S. Nagarajan, E. Ito, S. Y. Lee, Y. S. Kang, W. Choi, *Carbon* **2012**, 50, 4815.
- [15] W. Yang, X. Xu, Z. Tu, Z. Li, B. You, Y. Li, S. I. Raj, F. Yang, L. Zhang, S. Chen, A. Wang, *Electrochim. Acta.* **2015**, 173, 715.
- [16] D. H. Seo, S. Pineda, J. Fang, Y. Gozukara, S. Yick, A. Bendavid, S. K. H. Lam, A. T. Murdock, A. B. Murphy, Z. J. Han, K. Ostrikov, *Nat Commun.* **2017**, 8, 14217.
- [17] R. Muñoz, C. Gómez-Aleixandre, *Chemical Vapor Deposition* **2013**, 19, 297.
- [18] L. M. Malard, M. A. Pimenta, G. Dresselhaus, M. S. Dresselhaus, *Physics Reports* **2009**, 473, 51.
- [19] S. Niyogi, E. Bekyarova, M. E. Itkis, H. Zhang, K. Shepperd, J. Hicks, M. Sprinkle, C. Berger, C. N. Lau, W. A. de Heer, E. H. Conrad, R. C. Haddon, *Nano Letters* **2011**, 10, 4061.
- [20] S. Yick, Z. J. Han, K. Ostrikov, *Chem Commun* **2013**, 49, 2861.
- [21] X. Li, W. Cai, L. Colombo, R. S. Ruoff, *Nano Letters* **2009**, 9, 4268.
- [22] R. S. Weatherup, B. C. Bayer, R. Blume, C. Baetz, P. R. Kidambi, M. Fouquet, C. T. Wirth, R. Schlögl, S. Hofmann, *ChemPhysChem* **2012**, 13, 2544.
- [23] W. Wang, Y. Liu, Y. J. Zhong, L. Wang, W. Zhou, S. Wang, M. O. Tadé, Z. Shao, *Sol. RRL.* **2017**, 1, 1700074.
- [24] J. D. Roy-Mayhew, G. Boschloo, A. Hagfeldt, I. A. Aksay, *ACS Appl. Mater. Interfaces.* **2012**, 4, 2794.
- [25] M. Ye, X. Wen, M. Wang, J. Iocozzia, N. Zhang, C. Lin, Z. Lin, *Mater. Today.* **2015**, 18, 155.
- [26] D. D. Tune, B. S. Flavel, J. S. Quinton, A. V. Ellis, J. G. Shapter, *ChemSusChem* **2013**, 6, 320.
- [27] D. C. Marcano, D. V. Kosynkin, J. M. Berlin, A. Sinitskii, Z. Sun, A. Slesarev, L. B. Alemany, W. Lu, J. M. Tour, *ACS Nano.* **2010**, 4, 4806.